Supporting information

Underestimated charge storage capability in carbon cathode for advanced alkali-metal ion capacitors

Hong Tan [a], Xiuyi Lin [a], Jianqiu Huang [a], Jiaqiang Huang [a], Maijia Shi [a], Xiaoqiong Du [a], Biao Zhang [a,b] *

[a] *Department of Applied Physics, the Hong Kong Polytechnic University, Hung Hom, Hong Kong, P.R. China.*

[b] *The Hong Kong Polytechnic University Shenzhen Research Institute, Shenzhen, P.R. China.*

Corresponding author: Biao Zhang. Email: biao.ap.zhang@polyu.edu.hk

Experimental

1. Material preparation

The carbon materials were prepared through a two-step process. Firstly, lignin (low sulfonate content, Sigma Aldrich) was pre-carbonized at 600 ^{o}C for 1 h in argon atmosphere. The obtained products (LC-600) were then mixed with KOH pellets in a mass ratio of 1:4 by hand grounding in an agate mortar, following by annealing in a tubular furnace at 800/900/1000 ^{o}C for 2 h under argon protection with a ramp rate of 3 ^{o}C min^{-1}. Afterwards, the product was washed with diluted HCl solution and DI water to obtain the final activated carbon (LAC-800, LAC-900, LAC-1000). For comparison, an additional washing step was added after pre-carbonization at 600 ^{o}C to remove the impurities for probing their effects on the activation, as illustrated in Fig. 1, the obtained samples are marked as LCw-600. The following activation step

was kept identical and the final products are noted as LACw-900.

2. Material Characterization

The morphology of the samples and elemental composition of the electrodes were characterized using scanning electron microscopy and energy dispersive spectroscopy (SEM, EDS TESCAN VEGA 3). The X-ray diffraction (XRD) patterns were collected on Rigaku Smart Lab 9kW Diffractometer using Cu-Kα radiation (λ=1.54178Å). X-ray photoelectron spectroscopy (XPS) was taken on PHI5600 X-ray Photoelectron Spectrometer (Physical Electronics, Inc.) using a monochromatic Al Kα radiation at 14 kV. Nitrogen adsorption/desorption isotherms were measured to probe the surface area and porosity on a micromeritics ASAP 2020 machine. Raman spectra were obtained on a Witec-Confocal Raman system (UHTS 600 SMFC VIS) using laser with wave length of 532nm.

3. Electrochemical measurement

The electrodes consist of 80 wt.% active material, 10 wt.% conductive carbon black and 10 wt.% carboxymethylcellulose sodium binder. The mixtures were dispersed in DI water to prepare a slurry, which was coated on a copper foil for making the electrode tape. Discs in diameter of 12 mm were cut from the tape to employ as working electrodes in the LICs. Typical loading of each electrode was around 2.0 mg. Standard CR2032 coin cells were assembled in an argon-filled glove box with oxygen and water content lower than 0.5 ppm. For LIC assembling, the coin cell includes a Li foil as the counter electrode, the as-prepared electrode, the electrolyte composed of 1 M $LiPF_6$ in ethylene carbonate (EC)/dimethyl carbonate (DMC) (1:1 in volume) and

the glass fiber separator (Whatman, GF/D). 100 μL of the electrolyte was added to each cell. The performance of NICs and KICs were measured in the same configurations while the counter electrode was replaced by Na and K metal, respectively. The salt in the electrolyte was changed to $NaPF_6$ and KPF_6 accordingly, while their concentrations remain 1 M. The electrochemical performances of the cells were tested by galvanostatic cycling method on LAND CT2001A Battery Testing systems. The electrochemical impedance spectroscopy (EIS) was conducted on a SP150 (Biologic, France) workstation. Cyclic voltammetry (CV) curves were collected on an electrochemical workstation (Solartron Analytical 1400 cell test system) within 1.0-4.8 V at scan rates of 0.5, 1, 2, 4, 6, and 8 $mV \cdot s^{-1}$.

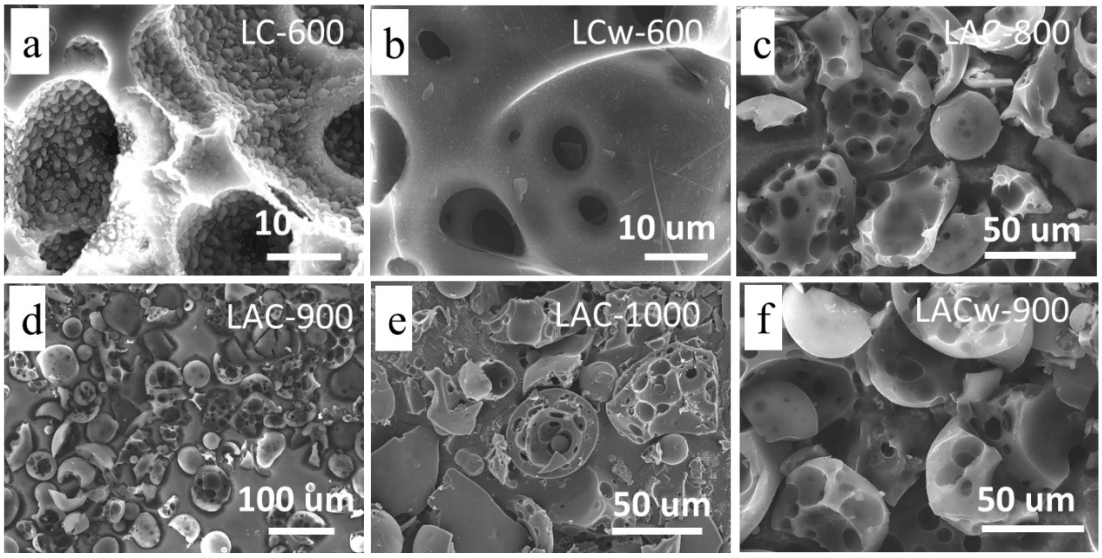

Fig. S1. SEM images for a) LC-600; b) LCw-600; c) LAC-800; d) LAC-900; e) LAC-1000 and f) LACw-900.

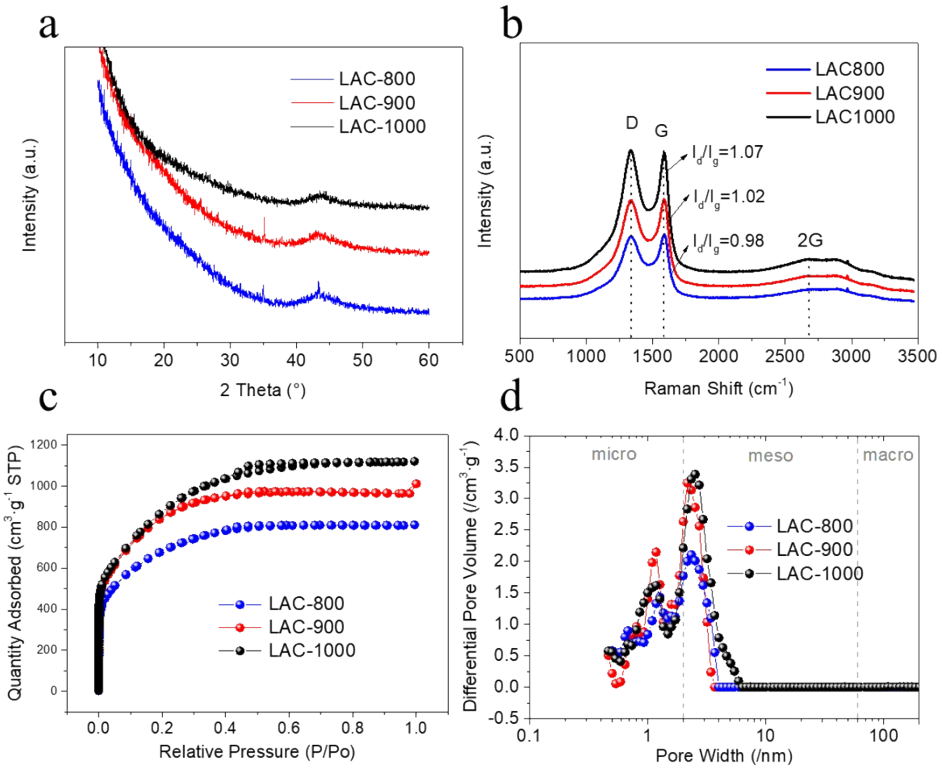

Fig. S2. Material characterization for LAC-800, LAC-900 and LAC-1000. a) XRD patterns; b) Raman spectra; c) N_2 adsorption/desorption curves and d) Pore distribution curves.

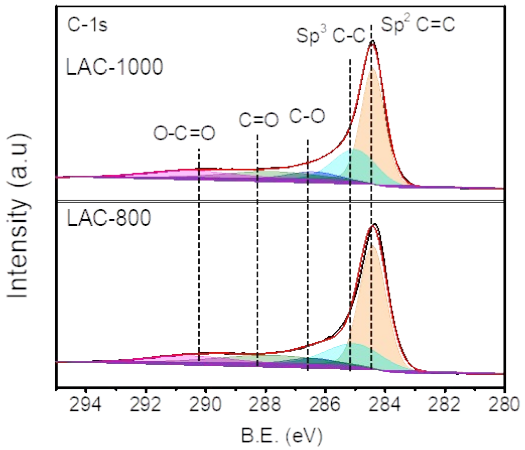

Fig. S3. XPS spectra of LAC-800, LAC-1000. XPS spectra indicate that most of the oxygen functional groups were removed and the sp^2 (C=C) structure content was largely increased after activation.

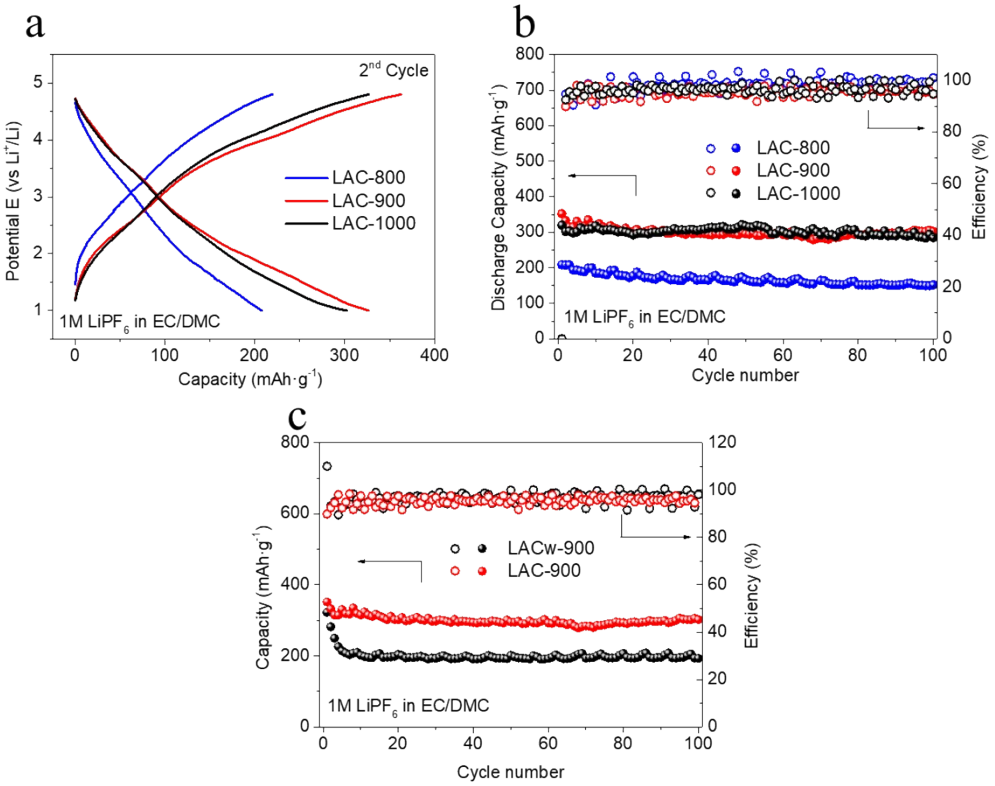

Fig. S4. a) Voltage profiles of 2nd cycle and b) Cycling test of LICs for LAC-800, LAC-900 and LAC-1000 both at 0.1 A·g^{-1}; c) Comparison of cycling test for LAC-900 and LACw-900 at 0.1 A·g^{-1}.

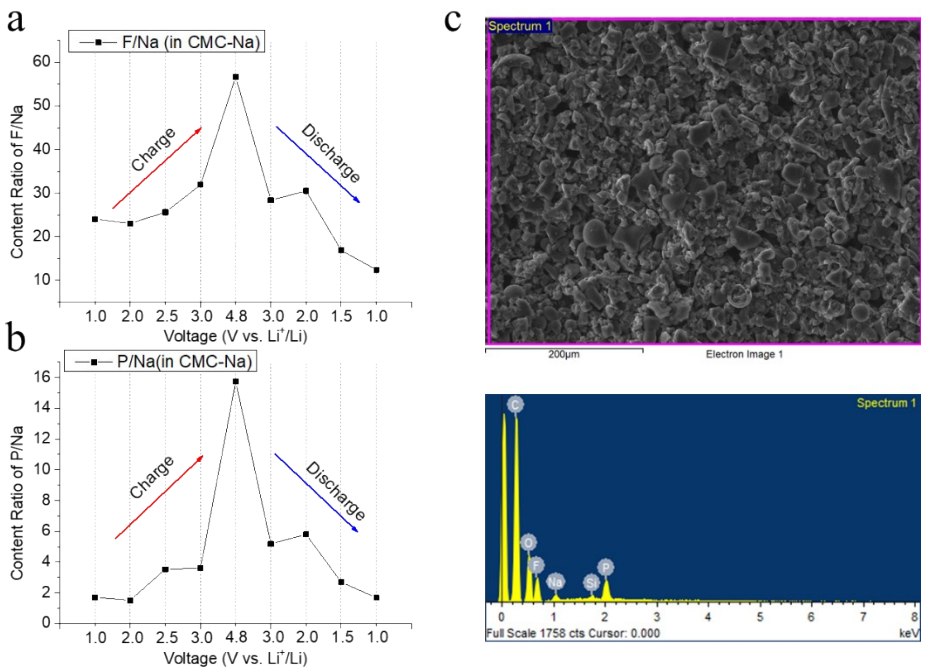

Fig. S5. EDS atomic ratio of (a) F/Na (in CMC-Na binder) and (b) P/Na (in CMC-Na binder) under various charge/discharge depth; Representative (c) SEM image and EDS spectra of the electrode.

For EDS tests, the cells were pre-cycled for three cycles before preparing the samples at different states. The batteries were disassembled in a glove box filled with ultra-pure argon and the electrodes were washed with DMC to remove the residual electrolyte. The Na content in the binder is used as a reference as it is not involved in the reaction.

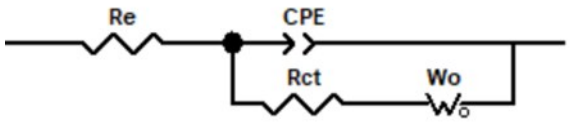

Fig. S6. Equivalent circuit for Nyquist plots fitting.

For electrochemical impedance spectroscopy (EIS) analysis, the equivalent circuit depicted in Fig. S6 was used to fit the original Nyquist plots[1]. In this model, Re represents the ohmic resistance of the electrolyte and the internal resistance of the electrode material, which corresponds to the first crossing point between the semicircle and the real axis. R_{ct} represents the interfacial charge transfer resistance, which refers to the impedance semicircle in high frequency and is the directive factor showing the impedance change at the solution-electrode interface.

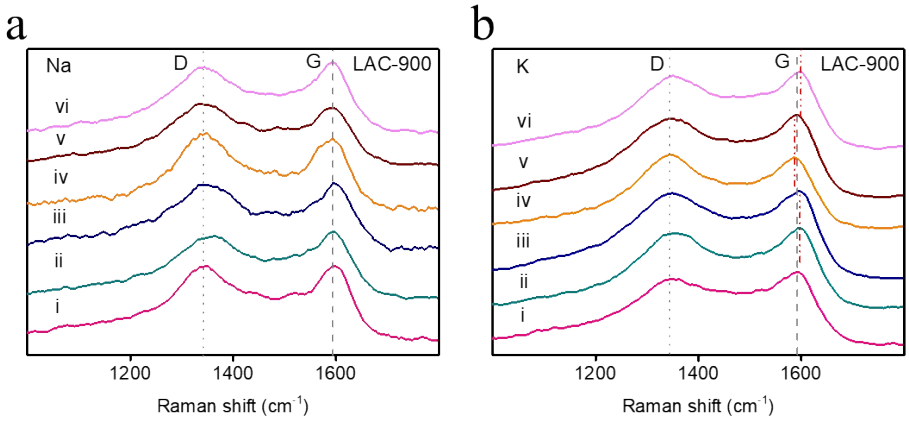

Fig. S7. In-situ Raman spectra of carbon cathode in (a) NICs and (b) KICs under various states: i) pristine; ii) charged to 4.8 V; iii) discharged to 3.0 V; iv) discharged to 1.0 V; v) charged to 3.0 V and vi) re-charged to 4.8 V.

The current separation method is used to analyze the surface capacitive behavior and bulk diffusion-controlled process of LAC-900. According to equation (1), the current can be divided into two parts at a certain potential: $k_1\nu$ represents capacitive contribution and $k_2\nu^{1/2}$ denotes diffusion-controlled contribution[2]. By dividing both sides of equation (1) with $\nu^{1/2}$, equation (2) is obtained. The values of k_1 and k_2 can be determined by plotting $i/\nu^{1/2}$ versus $\nu^{1/2}$, as shown in Fig. S5b.

$$i=k_1\nu + k_2\nu^{1/2} \text{——} (1)$$

$$i(V)/\nu^{1/2} = k_1\nu^{1/2} + k_2 \text{——} (2)$$

Thus, the capacitive contribution can be separated from the overall capacity, as depicted in Fig. S6c, with the orange-colored area representing its portion. At the scan rate of 0.5, 1.0, 2.0 and 4.0 $mV \cdot s^{-1}$, the capacitive contribution in LICs increases with the scan rate, accounting for 42.7%, 47.9%, 56.5% and 67.2% of the total capacity, respectively. The reasons lie in the slower kinectics of diffusion behavior than capacitive process, making the latter less rate-dependence.

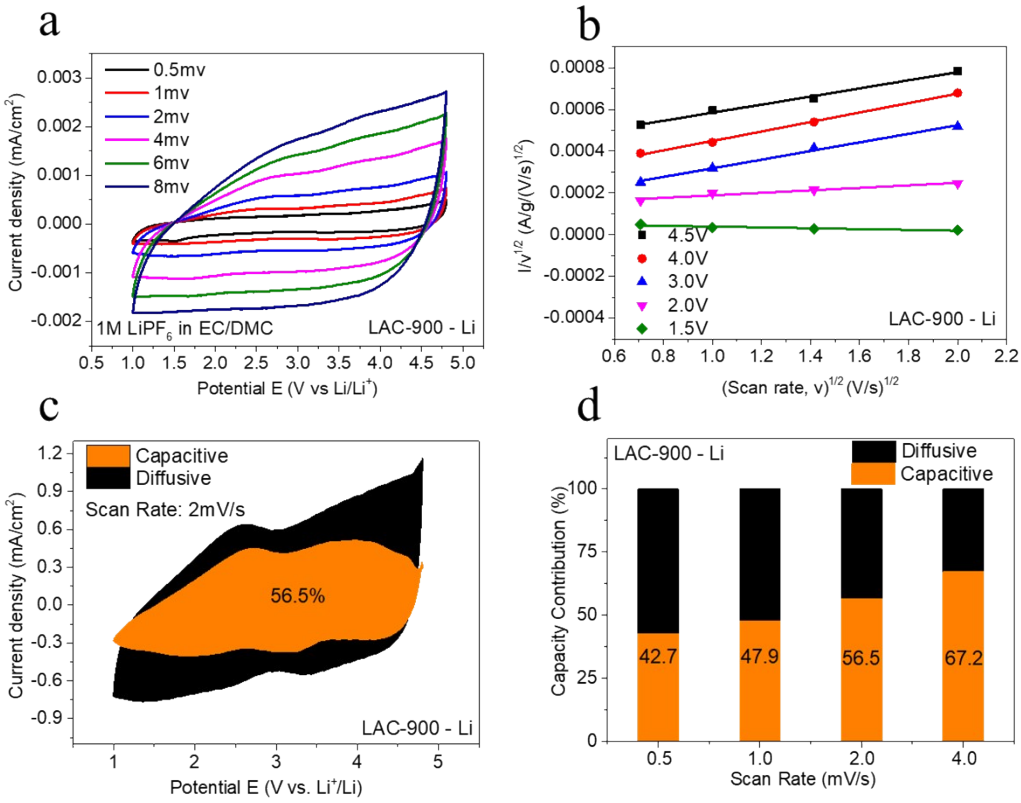

Fig. S8. CV test for LICs. a) CV curves of LAC-900 at different scan rates; b) Use of equation (1) to study the anodic voltammetry data for LAC-900 at scan rates from 0.5 to 8.0 mV; c) CV curves of LAC-900 with orange-shadowed area representing capacitive contribution; d) Column bars showing capacitive contribution under various scan rates.

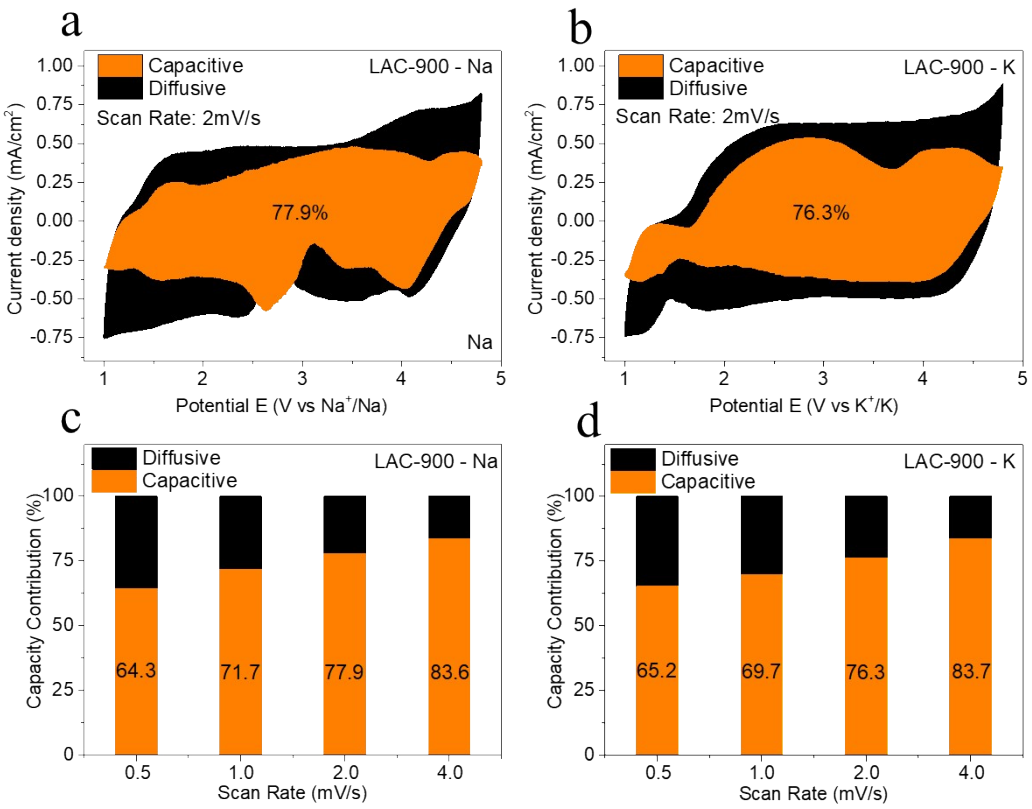

Fig. S9. CV curves of LAC-900 with orange-shadowed area representing capacitive contribution for a) NICs and b) KICs; Bar charts with orange colored portion denoting capacitive contribution under various scan rates for c) NICs and d) KICs.

Table S1. BET surface area, pore volume and average pore size for LAC-800, LAC-900, LAC-1000 and LACw-900.

	LAC-800	**LAC-900**	**LAC-1000**	**LACw-900**
S_{BET} (m^2/g)	2321	2880	3080	1829
Pore volume (cm^3/g)	1.2	1.6	1.7	0.95
Average pore size (nm)	2.2	2.2	2.3	2.1

Table S2. XPS analysis of element content of LC-600, LAC-800, LAC-900, LAC-1000.

Atom	Atomic Concentration %			
	LC-600	**LAC-800**	**LAC-900**	**LAC-1000**
Na	21.43	0.07	0.03	0.02
O	32.23	4.08	3.47	2.09
C	45.34	95.50	96.16	97.85
S	1.00	0.36	0.33	0.04

Table S3. XPS peak differentiation results given by area-related content ratio for different bonds.

Sample	Content %				
	Sp2 C=C	**SP3 C-C**	**C-O**	**C=O**	**O-C=O**
LC-600	27%	18%	14%	12%	29%
LAC-800	54%	20%	4%	13%	9%
LAC-900	53%	18%	7%	13%	9%
LAC-1000	50%	23%	6%	11%	4%

Table S4. R_{ct} values obtained from Nyquist plots fitting results.

Cut-off Voltage	4.8 V	3.0 V	2.0 V	1.5 V	1.0 V
R_{ct} (Ohm)	112	182	148	255	330

References

[1] Ge, H., Kong, Y., Pan, Y., Deng, L., Shou, D., & Lu, Q. (2015). Polydopamine core half-polyamidoamine dendrimers based drug-delivery platform and characterization by electrochemical impedance spectroscopy. *Journal of The Electrochemical Society*, 162(10), G87-G93.

[2] Wang, J.; Polleux, J.; Lim, J.; Dunn, B. (2007). Pseudocapacitive Contributions to Electrochemical Energy Storage in TiO_2(Anatase) Nanoparticles. *J. Phys. Chem. C*, 111 (40), 14925–14931.